Cell-Substrate Interactions and Locomotion of *Dictyostelium* Wild-Type and Mutants Defective in Three Cytoskeletal Proteins: A Study Using Quantitative Reflection Interference Contrast Microscopy

Mathias Schindl,* Eva Wallraff,‡ Barbara Deubzer,* Walter Witke,‡ Günther Gerisch,‡ and Erich Sackmann*
*Physics Department, Biophysics Group E22, Technische Universität München, D-85747 Garching, and ‡Max-Planck-Institut für Biochemie, D-82152 Martinsried, Germany

ABSTRACT Reflection interference contrast microscopy combined with digital image processing was applied to study the motion of *Dictyostelium discoideum* cells in their pre-aggregative state on substrata of different adhesiveness (glass, albumin-covered glass, and freshly cleaved mica). The temporal variations of the size and shape of the cell/substratum contact area and the time course of advancement of pseudopods protruding in contact with the substratum were analyzed. The major goal was to study differences between the locomotion of wild-type cells and strains of triple mutants deficient in two F-actin cross-linking proteins (α-actinin and the 120-kDa gelation factor) and one F-actin fragmenting protein (severin). The size of contact area, A_c, of both wild-type and mutant cells fluctuates between minimum and maximum values on the order of minutes, pointing toward an intrinsic switching mechanism associated with the mechanochemical control system. The fluctuation amplitudes are much larger on freshly cleaved mica than on glass. Wild-type and mutant cells exhibit remarkable differences on mica but not on glass. These differences comprise the population median of A_c and alterations in pseudopod protrusion. A_c is smaller by a factor of two or more for all mutants. Pseudopods protrude slower and shorter in the mutants. It is concluded that cell shape and pseudopods are destabilized by defects in the actin-skeleton, which can be overcompensated by strongly adhesive substrata. Several features of amoeboid cell locomotion on substrata can be understood on the basis of the minimum bending energy concept of soft adhering shells and by assuming that adhesion induces local alterations of the composite membrane consisting of the protein/lipid bilayer on the cell surface and the underlying actin-cortex.

INTRODUCTION

The role of the actin system in motile cells is being analyzed intensely by a variety of methods (Lee et al., 1993a). Among the physical methods applicable to living cells, micromechanical techniques have provided information on local force generation and elastic properties of the cell cortex (Kolodney and Elson, 1993; Harris et al., 1980; Evans, 1993). Another method, whose potential is not yet fully explored, is reflection interference contrast microscopy (RICM). Application of this technique to study cell contact with a substratum has been pioneered by Curtis (1964), and the technique has been converted into a quantitative tool by the theoretical work of Gingell and Todd (1979). In combination with fast image processing, RICM has been adapted to measure weak interaction forces between particles and surfaces (Rädler and Sackmann, 1992), to determine the bending elastic constants of membranes by spectroscopy of thermal flickering (Zilker et al., 1992), and to measure with high precision the optical thickness and separation distance of phospholipid bilayers at solid surfaces (Rädler and Sackmann, 1993).

The interpretation of physical data obtained with intact cells is complicated by the fact that similar viscoelastic properties of actin gels can be brought about in different ways. For instance, a given viscoelastic impedance may be indicative of a certain G- to F-actin ratio, a certain average polymer chain length, or of the presence of F-actin cross-linking proteins (Müller et al., 1991; Sackmann, 1994; Janmey, 1991). The difficulty of interpreting data obtained in vivo is accentuated by the large number of actin-binding proteins in a cell and the multiple control mechanisms thought to coordinate the activities of these proteins. Because of these complexities, a combination of genetic, biochemical, and physical methods appears to be the most promising approach to dissect the molecular network underlying the locomotion and interaction of cells with a substratum.

Locomotion of amoeboid cells in the microorganism *Dictyostelium discoideum* resembles the movement of vertebrate cells, particularly the highly motile mammalian polymorphonuclear leukocytes (Devreotes and Zigmond, 1988). As these white blood cells, *D. discoideum* cells respond to external stimuli by chemotaxis. This means that they are capable of transducing to the cytoskeleton signals received by cell-surface receptors, and to regulate locally the activities of cytoskeletal proteins in accord with the direction of an external concentration gradient of chemoattractant (Gerisch and Keller, 1981). Actin-binding proteins of *Dictyostelium* are surprisingly similar to proteins of vertebrate cells, as demonstrated by sequence relationships of proteins with corresponding functions (Noegel et al., 1989). *Dictyostelium* has the advantage that the complement of cytoskeletal proteins can be altered easily in its haploid cells by genetic techniques.

A number of mutants with specific defects in proteins of the actin system has been generated in *D. discoideum* and analyzed. One group of these mutants is altered in motor

Received for publication 29 August 1994 and in final form 5 December 1994.
Address reprint requests to Dr. Erich Sackmann, Physics Department-Biophysics Grp. E22, Technical University of Munich, James-Franck-Strasse, D-85748 Garching, Germany. Tel.: 49-89-3209-2471; Fax: 49-89-3209-2469; E-mail: sackmann@physik.tu-muenchen.de.

0006-3495/95/03/1177/14 $2.00

proteins. Lack of myosin II heavy chains causes cell locomotion to be slowed down. Only rudimentary capability to divide during mitosis is maintained in the myosin II null cells (De Lozanne and Spudich, 1987; Knecht and Loomis, 1987). Elimination of three phosphorylatable threonine residues at the heavy chains also reduces the speed of cell movement and forces the myosin to accumulate strongly in the cortex of the cells (Egelhoff et al., 1993; Gerisch et al., 1993). Lack of single members of the myosin I subfamily results in a decrease of phagocytotic activity by about 30% (Jung and Hammer III, 1990) or in alterations of cell motility (Titus et al., 1993). These effects are not as strong as myosin II defects, most likely because members of the myosin I subfamily can partially replace each other.

Actin-binding proteins other than motor proteins are considered to be important for the sol-gel transition of actin and for its coupling to the plasma membrane during cell locomotion (Taylor and Condeelis, 1979; Janmey et al., 1990; Müller et al., 1991; Ruddies et al., 1993; Isenberg and Goldmann, 1992). Among the regulatory proteins of *Dictyostelium* eliminated by mutation, the lack of coronin results in phenotypic changes that in some respect resemble those in myosin II null mutants (de Hostos et al., 1993). Compared with the myosin II and coronin deficiencies, the lack of one of the major actin cross-linking proteins, α-actinin (Wallraff et al., 1986; Witke et al., 1987; Schleicher et al., 1988) and 120-kDa gelation factor (Brink et al., 1990; Cox et al., 1992), or of the F-actin cutting protein severin (André et al., 1989) causes little harm to the cells. In the light of the activities of these three proteins in vitro, this has been unexpected. The activities of these proteins dominate those of any other cross-linking or, respectively, severing proteins in *Dictyostelium* cell homogenates (Condeelis and Vahey, 1982; Condeelis et al., 1984; Brown et al., 1982). These results have led to the view that essential functions of the actin system of *Dictyostelium* are guaranteed by the implementation of redundancy, that is by the presence of more than a single protein for a given function (Witke et al., 1992).

Because mutations that eliminate either α-actinin, 120-kDa gelation factor, or severin have only subtle effects, we have concentrated in this study on triple mutants that lack all three proteins together. The interaction of wild-type and mutant cells with a substratum was compared in quantitative terms using a refined RICM technique. In a first series of experiments, the smooth and strongly hydrophilic surface of mica was identified as an optimal substratum to detect variations in cell locomotion and adhesion by the RICM technique. Our next goal was to demonstrate the power of RICM combined with the use of mica and digital image processing in analyzing cell behavior in wild-type and mutant cells.

MATERIALS AND METHODS

RICM

The basic principle of image formation by RICM is illustrated in Fig. 1. Light waves reflected from a solid glass or mica surface (I_1) and from the ventral cell surface (I_2) interfere. The intensity distribution $I(\vec{r})$ in the image

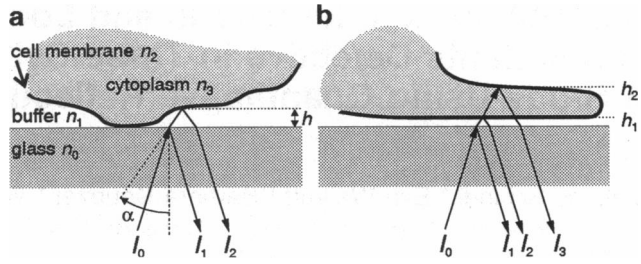

FIGURE 1 (*a*) Principle of RICM image formation. The image is formed by the interference of light reflected from the surface of the glass substratum with light reflected from cellular surfaces that are in a short distance from the substratum. Reflective surfaces correspond to steps in the refractive index n ($n_0 = 1.51$; $n_1 = 1.33$; $n_2 \approx 1.36$; $n_3 \approx 1.33$), and their reflectivity is proportional to the size of these steps. The maximum distance h that leads to visible interference decreases with increasing angle α of illumination aperture. (*b*) Small distance of ventral *and* dorsal membrane (h_1 and h_2) from the substrate surface leads to triple interference, which causes very dark appearance at portions of thin lamellipodial lobes in RICM.

plane of the objective is related to the local distance between surface of the substratum and cell approximately as

$$I(\vec{r}) \propto I_1 + I_2 + 2\sqrt{I_1 I_2} \cdot Y[\alpha, h(\vec{r})] \cdot \cos\left[\frac{4\pi n}{\lambda} \cdot h(\vec{r}) \cdot (1 - Z(\alpha)) + \delta\right] \quad (1)$$

according to Rädler and Sackmann (1993), where n is the refractive index of the buffer solution and λ is the wavelength of the illumination. The angle δ accounts for a phase jump of the light that is reflected at the buffer-cell interface, and is generally $\delta = \pi$ if a positive step in the refractive index is assumed. This explains why the contact area of adhering cells ($h \approx 0$) appears dark in RICM. The terms Y and Z both depend on the angle α of the illumination aperture. The value of Y falls with growing h and accounts for damping of higher order interferences. This limits the observed depth to some 100 nm above the substrate, strongly depending on α, i.e., the value of the illumination numerical aperture (INA). Therefore, the choice of the INA is a crucial point in RICM. It is necessary to find the best compromise between resulting light intensity and the error in $h(\vec{r})$ measurements that is caused by the deviation from parallel incidence (Gingell et al., 1982). Changing the INA during observation can reveal unknown object geometries.

Because the intensity of the reflected light at the membrane surface I_2 is in any case very small ($\sim 10^{-3}$ times incident intensity), stray light must be eliminated. This is achieved by use of the reflection contrast technique, i.e., by placing a set of crossed polarizers in the light path and a $\lambda/4$-plate on top of the objective (Ploem, 1975). The use of polarized light causes further problems when birefringent materials like mica are used as a substratum. They make the reduction of stray light by the reflection contrast technique less efficient, resulting in a loss of contrast. To minimize this effect, the mica sheets must be very thin.

In the case of simple or known object shape (i.e., spheres, vesicles or even red blood cells), $h(\vec{r})$ can be obtained by inverse cosine-transformation of the measured light intensity. Ambiguities are usually resolved with the known information on the topology of the object (Zilker et al., 1987). If high precision of the measured $h(\vec{r})$ is required, this elimination of ambiguities can still be a tedious task (Rädler and Sackmann, 1993). A first approximation may always start with the assumption of parallel incidence, which leads to

$$h(\vec{r}) = \frac{\lambda}{4\pi n} \cdot \arccos[I(\vec{r}) - I_1 - I_2]. \quad (2)$$

The obtained values will then be subject to several corrections leading to increased precision. However, in the case of living amoebae, the shape is mostly unknown and sometimes very irregular, and strong perturbations

of the interference pattern may arise at sites where intracellular organelles come in close proximity to the position of the plasma membrane adjacent to the substratum. The image can be obscured not only by interference with light reflected from these organelles but also from the dorsal cell surface, as shown in Fig. 1 *b*. This disturbance may be recognized with a change of the INA (Verschueren, 1985), and the spots caused by rapidly flickering organelles can be eliminated with time averaging. Nevertheless, in our experiments with *Dictyostelium* cells, a pure and precise reconstruction of $h(\vec{r})$ was rarely possible at selected locations on the circumference of the close contact. For quantitative evaluation, we have therefore concentrated on two-dimensional "footprints" of the cell, the contact area. It is recognized as the region with zero-order dark interference intensity (for exact definition see Results).

Microscope and digital image processing

The microscope used in the present work has been described in detail elsewhere (Zilker et al., 1987; Rädler and Sackmann, 1992, 1993). It consists of an Axiomat inverted microscope (Zeiss, Oberkochen, Germany), supplemented by nonstandard optical devices for variable additional magnification and for observing RICM and phase contrast images alternately or in parallel. We used it with a Zeiss Antiflex-Neofluar 63×/1.25 OIL objective. A high pressure mercury arc lamp (HBO100/W2, Osram) provides sufficiently high light density to allow the use of a small INA. The INA can be adjusted in a large range (lowest value 0.48) by variation of the diameter of a diaphragm in the Fourier plane of the illumination optical path. The green 546.1-nm line of mercury is isolated by a bandpass filter ($d\lambda$ = 5 nm, 85% peak transmission). This filter also eliminates ultraviolet light that would harm living cells. Heating is prevented by an infrared-filter (KG3, Schott, Mainz, Germany) in the light path.

The interference image was, with variable magnification, directly projected onto the chip of a CCD camera (HR-480, Aqua-TV, Kempten, Germany) with manually adjustable analog gain. The camera provides a European standard video signal (CCIR, 50 Hz-interleaved), which was either recorded on a 1/4-inch S-VHS video tape recorder (AG7350, Panasonic) or directly fed into a video digitizer for digitizing into 256 graylevels. Two different image-processing systems were used to analyze live images or recorded image sequences. Digitizing of tape-recorded sequences was improved by a digital time base corrector (FA310, For.A, Tokyo, Japan).

One of the systems used, the modular, real-time image processing system Maxvideo (Datacube, Peabody, MA) was used primarily for the analysis of time-dependent variations of the contact area and for video enhancement of the microscope images before recording. It is completely controlled by software programs developed in our laboratory, using the real-time operating system OS9–68k (Microware, Des Moines, IA). The second image-processing system was used for digital recording and analysis of real-time "movies," to reconstruct the changing surface profiles, and to determine contact angles, curvatures, and speed of pseudopod extension. This system is based on a Macintosh Quadra 950 (Apple Computer) equipped with an accelerated display adapter (Futura LX, E-Machines) and PixelTools Imaging boards (Perceptics, Knoxville, TN). Control is performed through Image VDM software (Perceptics), based on the public domain image analysis software NIH Image.[1] Image VDM 1.49, as available with complete source-code from Perceptics, was adapted to our needs by addition of several self-programmed routines.

Wild-type and mutant cells

Amoebae of the *D. discoideum* strain AX2, in this paper referred to as "wild type," were compared with four strains of triple mutants: GSA1, TP1, HG1397, and HG1434. Construction of the mutants is described in Fig. 2, and their genotypes are shown in Table 1.

Because the mutations in the α-actinin gene tended to revert by deletion of the vector sequences, an aliquot of mutant cells was cloned on agar plates in parallel to the RICM experiments, and colonies of the clones were assayed by immunoblotting (Wallraff and Gerisch, 1991), using the α-actinin-specific monoclonal antibody 47-62-17. Revertants never exceeded 0.5% of the cells used in the RICM measurements.

Cells of wild type and mutants were cultivated on standard medium agar plates together with *Klebsiella aerogenes* as bacterial food (Williams and Newell, 1976). For RICM recording, growing cells from the edge of a colony were suspended in cold 17 mM K-Na phosphate buffer (Sörensen), pH 6.0, washed 3 times by centrifugation to remove the bacteria, and resuspended in the buffer at a density of 1×10^7 cells per ml. 1-ml suspensions of the starving cells were shaken with 200 rpm on a rotary shaker in 2.2-ml Eppendorf tubes at 21°C for no longer than 6 h. The cells were washed once again to avoid coating of the mica surface by proteins that had been released from the cells, and the cell suspension was diluted with the buffer to about 10^6 cells per ml before transfer on surfaces. For experiments in which

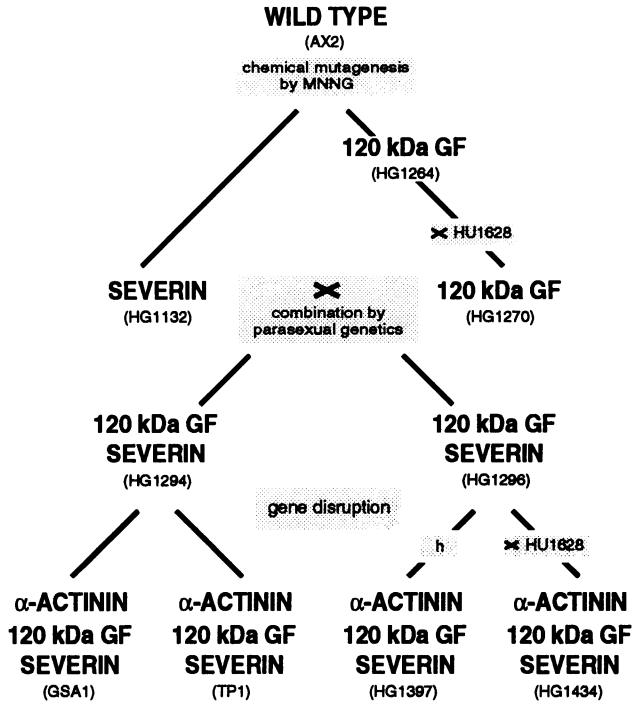

FIGURE 2 Construction of triple-mutant strains defective in the actin-binding proteins α-actinin, 120-kDa gelation factor, and severin. The diagram indicates in bold letters the mutations in cytoskeletal proteins, and in brackets the designation of the respective strains. Mutant HG1132 defective in severin (André et al., 1989) and mutant HG1264 defective in the 120-kDa gelation factor (Brink et al., 1990) were produced by chemical mutagenesis using 1-methyl-3-nitro-1-nitrosoguanidine (MNNG). The mutations in these strains were combined using the techniques of parasexual genetics (Newell, 1982). HG1264 was crossed with HU1628 to introduce selection markers that were needed for diploid selection. The two 120-kDa GF/severin double mutants that differ in their genetic background were transformed with a vector appropriate for disruption of the α-actinin gene (Witke et al., 1987, 1992). One transformant of HG1296 was subsequently crossed with HU1628 to alter extensively the genetic background by exchanging all the chromosomes that do not carry the cytoskeletal defects. During the construction of triple mutant HG1397 the original transformant of HG1296 became, for unknown reasons, spontaneously diploid, and was therefore haploidized (h) with thiabendazole (Welker and Williams, 1980). Genotypes of all triple mutants used in this paper are shown in Table 1.

[1] Written by Wayne Rasband at National Institutes of Health and available electronically via Internet by anonymous ftp from zippy.nimh.nih.gov or from Library 9 of the MacApp forum on CompuServe and on floppy disk from NTIS, 5285 Port Royal Rd., Springfield, VA 22161; part number PB93–504868).

TABLE 1 Genotypes of the four triple-mutant strains used in RICM measurements

	Linkage groups						
	I	II	III	IV	VI	VII	
GSA1	***gelA1000*** ***abp-tr(1)***	*axeA2* *axeC2*	*axeB2*	+	*manA2*	***sevA1000***	*cob-354*
TP1	***gelA1000*** ***abp-tr(2)***	*axeA2* *axeC2*	*axeB2*	+	*manA2*	***sevA1000***	*cob-354*
HG1397	***gelA1000*** ***abp-tr(3)***	*axeA2* *axeC2*	*axeB2*	+	+	***sevA1000***	+
HG1434	***gelA1000*** ***abp-tr(4)***	*acrA1823* *axeA1* *axeC1*	*bsgA5*	*whiC351*	*manA2*	***sevA1000***	*cob-354*

The linkage groups correspond to the seven chromosomes of haploid *D. discoideum* cells. (Linkage group V has not been labeled in the strains used for these experiments.) The dominant cobalt resistance mutation (*cob-354*) is associated with the endogenous extrachromosomal Ddp1 plasmid (Williams, 1978; Metz et al., 1983). Identical linkage group markers indicate presence of the same chromosome in the respective strains (if mutations that may have occurred spontaneously are neglected). Bold symbols indicate mutations in cytoskeletal proteins: *gelA1000* = defect in 120-kDa gelation factor (Brink et al., 1990); *abp-tr* = defect in α-actinin produced by transformation (Witke et al., 1987; Witke et al., 1992); *sevA1000* = defect in severin (André et al., 1989). For explanation of the remaining genetic markers, see Wallraff et al. (1984).
The table shows that triple mutants GSA1 and TP1 have the same genetic background. This is because they are transformants of the same parent strain, HG1294 (Fig. 2). HG1434 differs from these strains with respect to linkage groups II, III, and IV; HG1397 with respect to linkage group VI and the absence of cobalt resistance.

cAMPS was applied, the Sp-isomer of cyclic adenosine-3′,5′-monophosphothioate (Boehringer Mannheim, Mannheim, Germany) was used.

Substrata

Surfaces to which cells were exposed comprise clean glass, glass coated with human serum albumin (HSA), and freshly cleaved mica. Standard microscopic glass coverslips (24×24 mm, $d = 0.17$ mm) were thoroughly cleaned with ethanol and dried in a nitrogen flow. As shown by atomic force microscopy, these glasses possess rough surfaces on a nanometer scale (Radmacher, 1991). For coating, cleaned coverslips were immersed for 5 min into a solution of 0.2% HSA, which adsorbs to the surface and blocks sites to which the cells would strongly adhere.

Mica is a complex layered silicate. The layer structure of the common muscovite ($KAl_2(Si_3Al)O_{10}(OH,F)_2$), which has been used for this work, consists of an octahedral arrangement of aluminium ions, embedded in two tetrahedral layers of silicon and aluminum. Chemical bonds are formed via OH-groups. These triple layers are interconnected through a weakly bound film of interlayer cations, usually potassium ions. This film is responsible for easy cleavage of mica (Bayley, 1984). In aqueous surroundings, the potassium ions become hydrated and dissolve, leaving behind a very smooth and clean surface as visualized with atomic force microscopy (Radmacher, 1991). Because of exposed O^- ions, the surface is negatively charged and strongly hydrophilic.

The mica was split manually into sheets of 5- to 10-μm thickness using two sharpened forceps. These sheets were supported by an underlying glass coverslip. Matching of the refractive index with immersion oil ($n = 1.518$, Zeiss) was required between objective and glass and also between the glass surface and the thin mica sheet. Only freshly cleaved mica sheets were used, to guarantee a clean and smooth surface, which is essential for low adhesiveness.

Cell size measurements

To exclude that differences in the size of the contact area A_C are due to differences in cell size between wild-type and mutant strains, cells of the AX2, GSA1, and HG1397 strains were compared. Light scattering of single cells was determined as a measure of cell size using a FACS IV cell sorter (Becton Dickinson, San Jose, CA). No significant difference between AX2 and GSA1 was found (average peak positions of scattering differed by 2%). Scattering of HG1397 cells was about 30% higher than that of AX2 cells, indicating a larger (rather than smaller) cell size in this mutant.

RESULTS

Adhesion of *Dictyostelium* cells to different substrata

Preliminary studies revealed that cells of the *D. discoideum* wild-type strain AX2 adhere strongly to clean surfaces of glass and move only slowly on this substratum. The cells had difficulties detaching from the glass, leaving behind membrane material from retraction fibers, which by RICM is recognized as a track of black spots (Fig. 3 *a*). Furthermore, at the boundaries of contact areas the angle between the substratum and the cell surface was large, as indicated by the absence of interference fringes. By coating with HSA, the glass became less adhesive, as inferred from the appearance of several, clearly distinguishable interference fringes (Fig. 3 *b*). Freshly cleaved mica was the least adhesive material investigated, as deduced (i) from the multiple interference fringes extending from the contact area, indicating a small angle between cell surface and mica (Fig. 3 *c*), and (ii) from the absence of any detectable membrane material deposited on the mica.

Temporal changes in the size A_C of the contact area

To measure the contact area of single cells with solid surfaces, a high illumination numerical aperture (INA > 1.0) is required for RICM to obtain a sufficiently homogeneous dark area where the cells are in close contact with the substratum. To determine the size A_C of this area, the RICM images were processed as explained in Fig. 4. A_C was measured repeatedly at intervals of either 1 or 2 s for a period of 5–12 min.

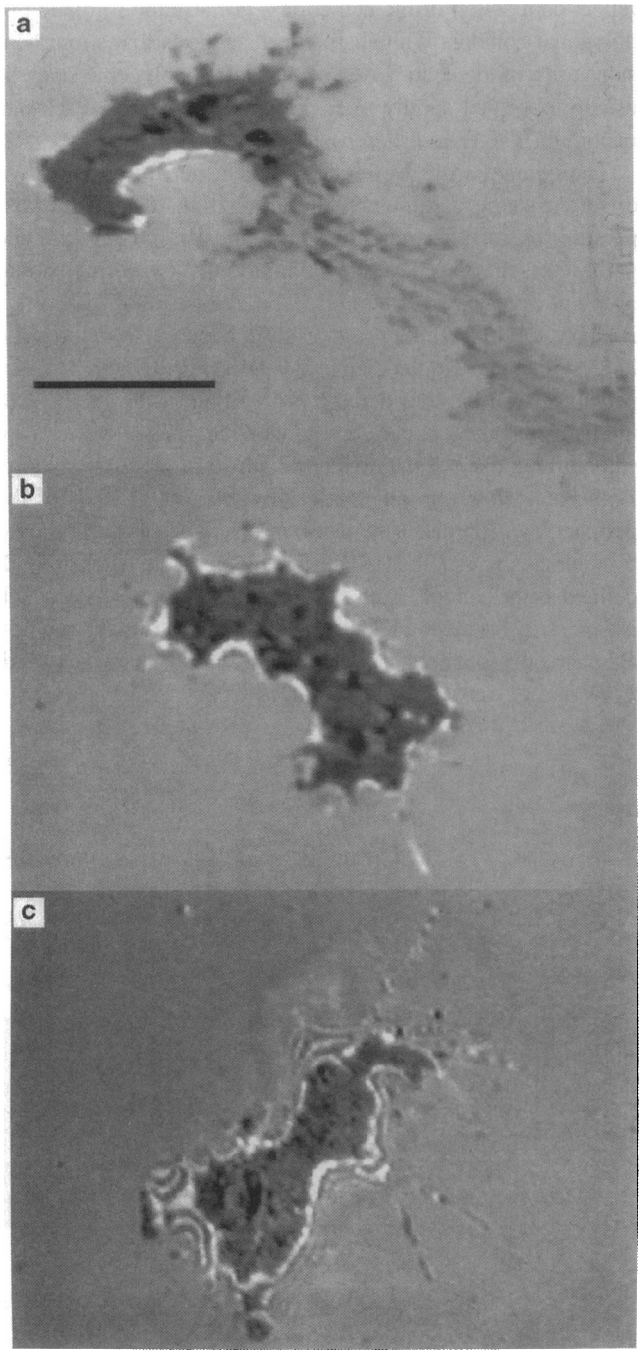

FIGURE 3 RICM images of *D. discoideum* wild-type cells on different substrata (bar indicates 10 μm). (*a*) On a substratum of clean glass, interference fringes are visible only at restricted regions of the rim, and a substantial amount of lost membrane material is visible as a track of black spots behind the moving cell. This points to strong adhesiveness. (*b*) On HSA-coated glass, the first-order interference fringe is visible along almost the entire rim of the contact area, pointing to a much weaker adhesiveness than on pure glass. (*c*) On freshly cleaved mica, the contact area is surrounded by multiple interference fringes, indicating a gentle sloping of the membrane distance *h* around the close contact. This points to a very weak adhesiveness.

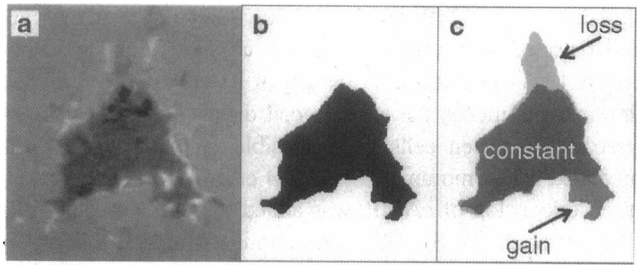

FIGURE 4 Consecutive steps of image processing for analysis of the contact area and its changes. (*a*) The typical RICM image of a *D. discoideum* wild-type cell, on HSA-coated glass or on mica, shows a dark area of close contact and interference fringes in the border region. Dark spots represent attachment sites of pseudopods or retraction fibers. (*b*) To distinguish the areas of close contact from other regions, images like that in (*a*) have been binarized with an appropriate threshold value, and the binarized images were further processed in three steps: (i) binarization noise was removed, (ii) holes completely surrounded by the area of close contact were filled, and (iii) single spots smaller than a given threshold size were removed. A field of observation with a size of 65 × 45 μm included up to four cells. Their contact areas were separated semi-automatically by the MAX-VIDEO image processing system under continuous visual control. The result defines the contact area of the cell; its size is called A_C. (*c*) To visualize and measure the gain, loss, and constant fraction, successively recorded contact areas processed as in (*b*) were compared with each other by an overlay technique.

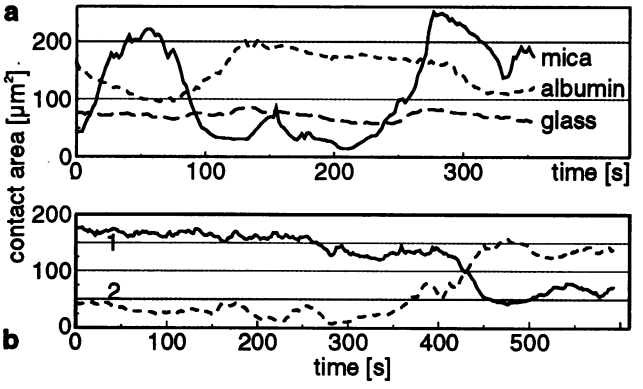

FIGURE 5 Temporal changes in the size A_C of the contact area of wild-type cells. (*a*) Fluctuations of A_C occurred on a time scale of minutes with small amplitudes on clean glass, intermediate amplitudes on HSA-coated glass, and high amplitudes on mica. (*b*) Changes in A_C on HSA-coated glass in the presence of 1 μM cAMPS, a blocker of cAMP-mediated cell communication. cAMPS was added to the cell suspension at 1 h before the experiment. The A_C recordings of two cells show that A_C still fluctuates in the presence of cAMPS.

Changes of A_C within the time scale of minutes were found for cells attached to all three of the surfaces examined (Fig. 5 *a*). On clean glass, A_C fluctuated only with small amplitudes, on HSA-coated glass the amplitudes were larger, and they were extremely large on mica. These findings parallel the different strengths of cell adhesion to the three surfaces, and thus suggest that strong adhesion prevents the cells from changing their area of contact.

The aggregation stage is initiated in *D. discoideum* by the pulsatile release of cyclic adenosine-3′,5′-monophosphate (cAMP), and the cells respond to these signals by a shape change called "cringing" (Futrelle et al., 1982; Wessels et al., 1989). Therefore, the question arises whether the A_C fluctuations are elicited by intercellular

signaling. The cAMP signals are known to be transmitted over a distance of 50 μm from one cell to another (Cohen and Robertson, 1971). Because at the density of 10^5 cells per cm^2, as used in our experiments, the average cell distance was 30 μm, interactions between cells were possible. To suppress cAMP-mediated cell communication, 1 μM cAMPS, a slowly hydrolyzed thioanalog of cAMP, was added to desensitize the cells (Rossier et al., 1978). This concentration of cAMPS was sufficient under our conditions to inhibit cell aggregation, which in the absence of cAMPS occurred within a few hours after transfer of the cells to a substratum. Fig. 5 *b* shows for two cells on HSA-coated glass that cAMPS did not abolish the A_C fluctuations, indicating that these fluctuations are caused by intrinsic changes in the state of single cells. A_C, as monitored on weakly or moderately adhesive surfaces, sensitively reflects these intrinsic changes.

Correlations between changes in the size and shape of contact areas

Fluctuations in the size of the contact area were accompanied by characteristic changes in its geometry. As shown in the micrographs of Fig. 6 *a*, three characteristic states could be distinguished in wild-type AX2 cells. (i) In an upright state, the cells exhibit a small and often discontinuous contact area (Fig. 6 *a1*). (ii) In a locomotive state, semi-circular fronts of the contact area are distinguishable that rapidly move forward (Fig. 6 *a2*). In this state, cells have often two fronts that advance in opposite directions, leading to a bipolar dumb-bell shape (Fig. 6 *a3*). (iii) A resting state is characterized by a large contact area that often assumes a polygonal shape (Fig. 6 *a4*). This shape appears to reflect contraction of the cell cortex, because the formation of polygonal contours with sharp edges suggests that strong tensions arise in the actin cortex of the cell. A polygonal shape is usually observed shortly after the contact area has reached a maximum size (Fig. 6 *b*, *top*).

The contact areas were classified further in terms of two different shape parameters, the elongation, E, and the dispersion, D, as introduced by Dunn and Brown (1990). The parameters are based on the calculation of two-dimensional moment invariants of the area. The elongation E characterizes the circular anisotropy or stretchedness. E relates the longest diameter l to the diameter b perpendicular to l. The dispersion D can be considered the deviation in the moment of inertia from the ideal ellipse with elongation E. D is low for a smooth boundary of the area and high for a folded periphery. Both parameters are rather insensitive to small details of the periphery, which makes them also insensitive to artifacts caused by digitization. Another useful parameter is the extension, $\mathcal{E}$, defined as the sum of E and D (Dunn and Brown, 1990), which is a measure for the total deviation of the shape from circularity. $\mathcal{E}$ is zero only for an exact circle. When l, b, and A_C are measured, E, D, and $\mathcal{E}$ can be directly obtained from

$$E = \log_2\left(\frac{l}{b}\right), \tag{3}$$

$$D = \log_2\left(\frac{\pi l b}{A_C}\right), \tag{4}$$

$$\mathcal{E} = D + E. \tag{5}$$

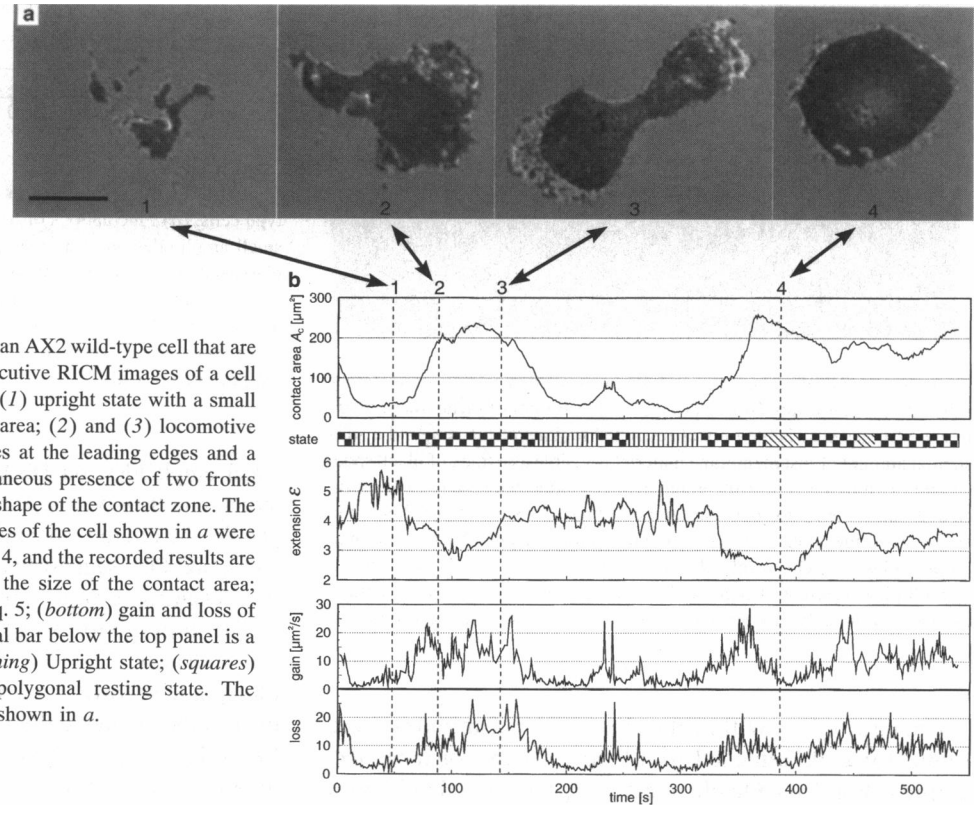

FIGURE 6 Fluctuations in the shape of an AX2 wild-type cell that are associated with changes in A_C. (*a*) Consecutive RICM images of a cell migrating on mica show different states. (*1*) upright state with a small and (in this case) discontinuous contact area; (*2*) and (*3*) locomotive states showing wide-spread contact zones at the leading edges and a dumb-bell shape produced by the simultaneous presence of two fronts in (*3*); (*4*) resting state with a polygonal shape of the contact zone. The bar indicates 10 μm. (*b*) The RICM images of the cell shown in *a* were processed as outlined in the legend of Fig. 4, and the recorded results are shown for a period of 9 min. (*top*) A_C, the size of the contact area; (*middle*) the extension $\mathcal{E}$ as defined in Eq. 5; (*bottom*) gain and loss of A_C as illustrated in Fig. 4 *c*. The horizontal bar below the top panel is a diagram of the cell states. (*vertical hatching*) Upright state; (*squares*) locomotive state; (*diagonal hatching*) polygonal resting state. The dashed vertical lines refer to the images shown in *a*.

A relationship between the extension, $\mathcal{E}$, and A_C of individual cells was revealed by plotting both parameters as a function of time. As shown in Fig. 6 *b*, large values of $\mathcal{E}$ (*middle*) corresponded to small values of A_C (*top*). By superimposing the contact areas of two successive images, the newly formed contact ("gain") and the area of detachment ("loss") can be quantified. Fig. 6 *b* (*bottom*) shows a correlation between gain and loss during periods of cell movement.

The temporal changes of the cell shape can also be characterized by plotting the variations of E and D with time as a path in an E-versus-D-plane (Fig. 7). No significant correlations between E, D, or $\mathcal{E}$ on one hand and the speed of cell movement on the other were observed.

Reduced size of contact areas for triple-mutant cells on mica

The data obtained by the RICM technique with wild-type cells were compared with data obtained with cells of triple mutants that lack three cytoskeletal proteins: the two F-actin cross-linking proteins α-actinin and 120-kDa gelation factor (ABP 120), and the F-actin fragmenting protein severin. Because of the possibility that the genetic background influences the result, four strains of triple mutants were included in this study that represent three different combinations of genetically marked chromosomes (Table 1). The genealogy of these mutants is outlined in Fig. 2.

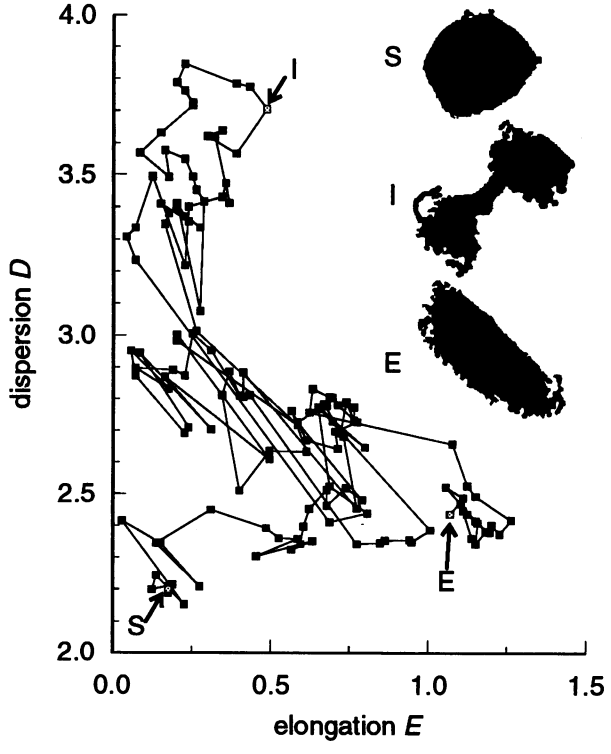

FIGURE 7 Phase diagram for the topology of the contact area. The path in the E-versus-D space starts at the point marked with "S" and ends at the point marked with "E." The data are from a 140-s section of the record shown in Fig. 6, corresponding to seconds 399 to 538 of that run. The insets show the binarized shape of the cell's contact area at the starting point (S), the end (E), and an intermediate time (I), visualizing the topology that leads to the measured values for E and D.

In an attempt to uncover differences between cells of wild-type and triple mutants in quantitative terms, we have determined the sizes of contact areas of these cells on an appropriate substratum. Whereas no obvious differences in A_C of wild-type and mutant cells were observed on glass (clean as well as HSA-coated), the weakly adhesive mica surfaces were optimally suited to elucidate such differences. Therefore, A_C values for randomly chosen single cells of wild-type and mutant strains were measured on this substratum (Fig. 8). In wild-type cells, the A_C values showed a broad, asymmetrical distribution, which is in accord with the large amplitude of temporal fluctuations on mica surfaces as illustrated in Fig. 6. In all four mutants, the median A_C values were lower than in the wild type and the distributions were more compressed (Table 2). As pointed out in Materials and Methods, the differences in A_C values cannot be attributed to cell size differences between wild-type and mutant strains. Statistical analysis showed that all data sets for mutants were different from the wild-type AX2 set. In three of the mutants, the sizes of contact areas were similar to each other. In the fourth mutant, HG1397, they were significantly smaller (Table 2), which suggests the existence of an additional mutation in HG1397.

The A_C values given in Fig. 8 are collected randomly from all states of the cells. As shown in Fig. 6, A_C values fluctuate in wild-type cells considerably with time. Consequently, differences between wild type and mutants can arise in one of two ways (or in a combination of both). One is that the mutant cells, rather than fluctuating, are arrested in the upright state at which A_C is small even in wild-type cells. Another possibility is that the mutant cells fluctuate, but within a range of A_C values smaller than for wild type. To distinguish between these possibilities, RICM images of single HG1397 cells were recorded on mica over a period of time. This mutant was chosen because it showed the strongest deviation of A_C values from wild type among all the mutants tested (Fig. 8). The mutant cells showed fluctuations, but they were shifted to a smaller range of A_C sizes (Fig. 9).

In HG1397 as well as in the other triple mutants, the same three different states as in wild-type cells were found (Figs. 6 and 9). In addition, a characteristic "blebbing" state was observed in the mutants, which usually occurred after the cells had passed the upright state and lasted for up to several minutes. In the blebbing state, the cells rapidly and frequently extended rounded pseudopods in all directions with essentially no net motion (Fig. 10).

Dynamics of lamellipod protrusions in wild-type and mutant cells

Locomotion of a cell is brought about by the combined action of pseudopods, either protruded simultaneously or consecutively. RICM can be used to measure the time course of pseudopod expansion in contact with a substratum. Here we have used RICM to compare lamellipods as they are formed

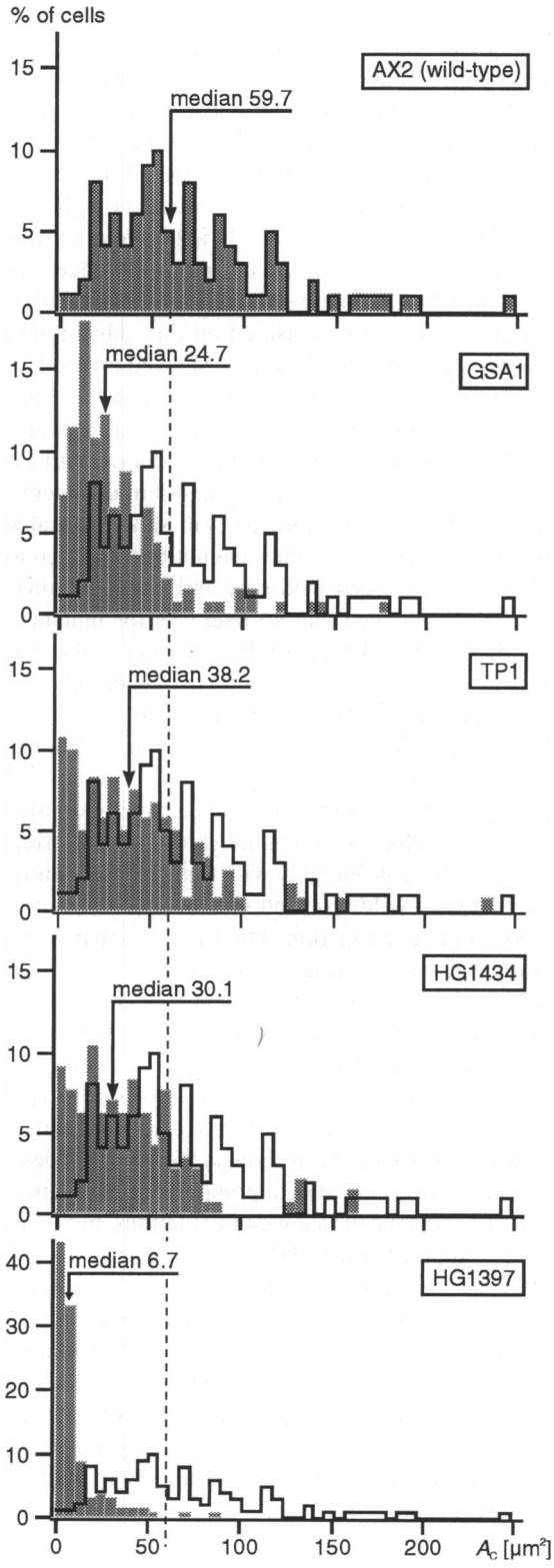

FIGURE 8 Reduced size of contact area A_C of mutant cells on mica. Normalized histograms of A_C are shown for cells of wild type AX2 and four triple-mutant strains. Each vertical bar covers an interval of 5 μm^2. The outlines in the histograms of mutants refer to the wild-type distribution. (Note that for the histogram on bottom the scale of the ordinate has been changed.) Median values are indicated for all distributions; the dashed line indicates the median of the wild-type distribution. Differences between wild type and all mutants proved to be significant with $p < 0.001$ using the nonparametric Mann-Whitney U-test.

TABLE 2 Distributions of A_c values for wild-type and triple-mutant strains on mica

Cell strain	A_c (μm^2) Median	*Iq.** 25	*Iq.** 75	Number of cells
AX2 (wild type)	59.7	39.9	91.5	105
GSA1	24.7	13.4	41.8	140
TP1	38.2	16.1	59.6	121
HG1434	30.1	13.3	52.2	145
HG1397	6.7	4.3	11.1	142

*The interquartiles *Iq* at 25 and 75% of the sorted A_c values are a measure of the width and asymmetry of the distributions.

in the locomotive state of wild-type and mutant cells in contact with mica. Lamellipods protruded into the free fluid space were not recognized by RICM. But those expanding in contact with mica (or HSA-coated glass) did so over their entire length up to the leading edge as judged from parallel observations with phase-contrast microscopy and RICM.

The lamellipods were free of intracellular particles and were thin with a sharp transition to the central portion of the cell. The RICM images often showed stripes or "leopard" patterns of dark and bright areas on the lamellipods, indicating local variations in the distance between cell surface and substratum. The leading edge often appeared darker than other areas, which is probably not caused by closer attachment but by flattening of the edge zone, as explained in Fig. 1 *b*.

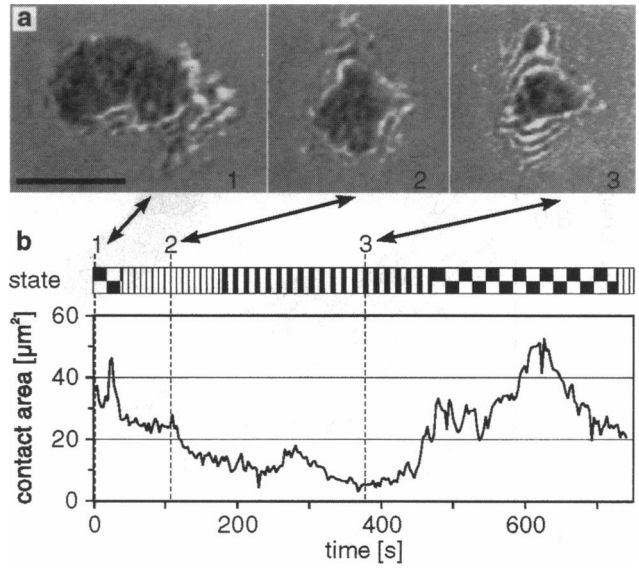

FIGURE 9 Fluctuations in the shape of a mutant HG1397 cell associated with changes in A_C. RICM images of the mutant cell were recorded on mica in analogy to the wild-type cell of Fig. 6. (*a*) RICM images showing the cell in three different states. (*1*) locomotive state, (*2*) upright state, and (*3*) blebbing state. The bar indicates 10 μm. (*b*) A_C plotted for a period of 12 min. The horizontal bar on top indicates the states of the cell. (*squares*) Locomotive state; (*vertical hatching*) upright state; (*bold vertical hatching*) blebbing state. The dashed vertical lines refer to the images shown in *a* (note that the scales in *b* are changed relative to Fig. 6).

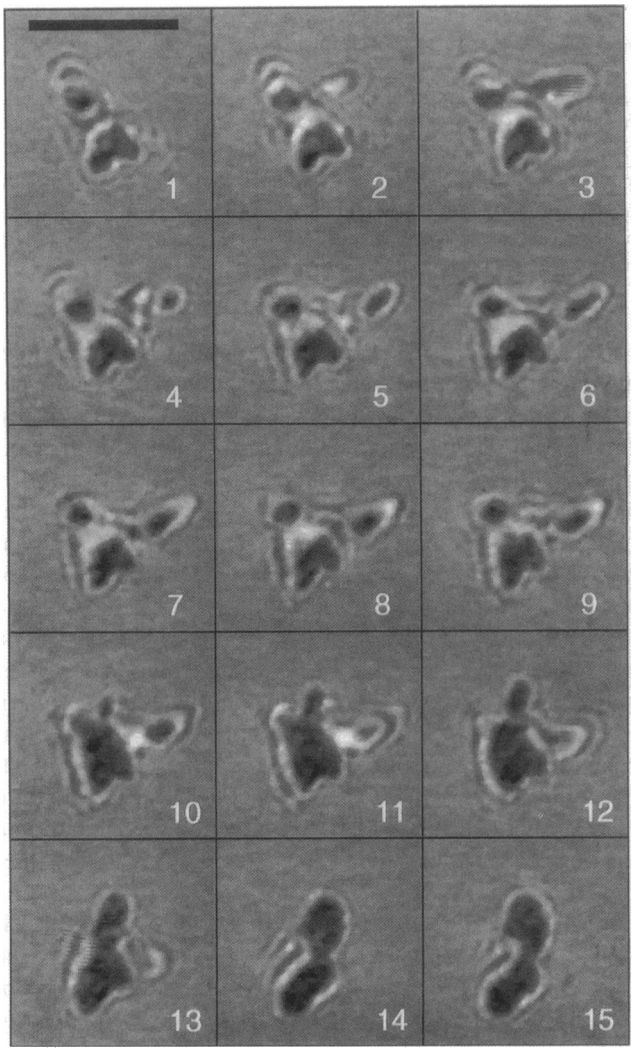

FIGURE 10 RICM images illustrating the blebbing state of a triple-mutant cell. A cell of mutant GSA1 was recorded on mica at short intervals of $\Delta t = 0.44$ s for a total period of 6.2 s. During this period, a bleb in the 2 o'clock direction was projected and retracted. Its retraction was accompanied by protrusion of another bleb in the 7 o'clock direction (frames 12–15).

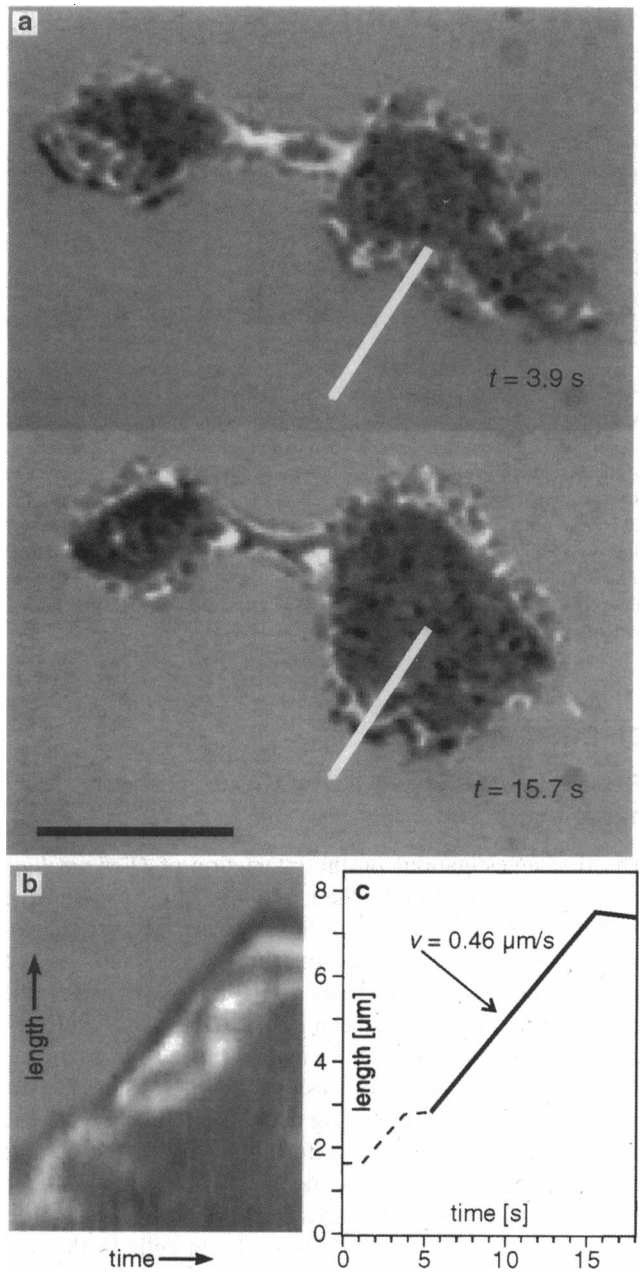

FIGURE 11 Lamellipod expansion in a wild-type AX2 cell in contact with a mica surface. The figure illustrates how tape recordings of cells in the locomotive state were analyzed. With the PixelTools-System (see Materials and Methods) regions of real-time or time-lapse videos containing a single cell were digitized. By replay, a linear cross section was marked along the axis of an expanding lamellipod, and movement of the front of the lamellipod along this line was measured. (*a*) Two RICM images of one cell recorded at an interval of 11.8 s. The dark rim of the contact area can be used to measure progression of a lamellipod that expands in contact with the substratum. The white line indicates the direction into which the contact area expands. The black bar indicates 10 μm. (*b*) Intensity profiles were recorded along the white line of (*a*) at intervals of $\Delta t = 0.28$ s and plotted versus time. In this synthetic image, the individual intensity profiles are plotted in vertical direction. The front of the lamellipod is clearly detectable; its slope gives the speed v. (*c*) Plot extracted from (*b*) showing the progression of the tip of the lamellipod. The plot illustrates abrupt start and stop of lamellipod formation and linear expansion in between.

Both in wild-type and mutant cells, lamellipod expansion commenced and ceased abruptly, and proceeded between start and stop with nearly constant speed (Figs. 11 and 12). Quantitative analysis revealed significant differences between AX2 and HG1397 cells in the speed and duration of expansion (Table 3). In the mutant, lamellipods were extended more slowly and for a shorter time than in the wild type. These differences resulted in a distance of expansion of single lamellipods in the mutant that was only about half of that in the wild type. Finally, a detail should be mentioned that might shed light on mechanisms of control. Statistical analysis revealed significant correlations between speed and duration of lamellipod expansion: the faster a lamellipod expanded, the shorter the expansion persisted. This correlation, observed both in AX2 wild type and mutant HG1397, suggests that it is the distance that is controlled.

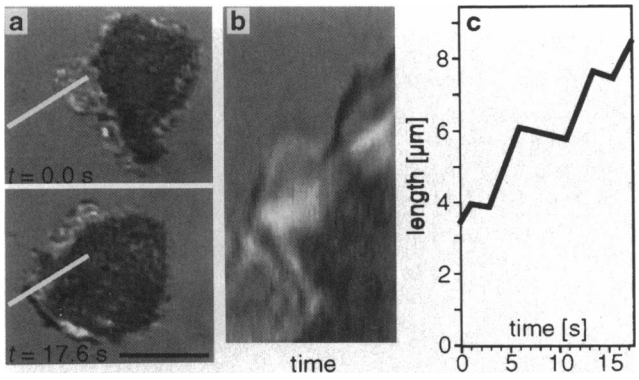

FIGURE 12 Lamellipod expansion in a mutant HG1397 cell in contact with a mica surface. The cell was in the locomotive state and analyzed analogous to the wild-type cell shown in Fig. 11. (*a*) Two RICM images of the same cell recorded at an interval of 17.6 s. The white line indicates the direction along which protrusion was measured. The black bar indicates 10 µm. (*b*) Intensity profiles along the white line in *a* were plotted versus time as in Fig. 11 *b*. (*c*) Movement of the front of lamellipods as taken from (*b*). The plot illustrates that expansion was linear and started and stopped abruptly as in wild-type cells, but phases of expansion were shorter in time and space.

TABLE 3 Median values for lamellipod expansion in cells of wild type AX2 and triple mutant HG1397

	Distance (µm)	Duration (s)	Speed (µm/s)
AX2	6.29	14.1	0.47
HG1397	2.86	10.7	0.34

Twenty lamellipods expanding in contact with a mica surface were analyzed for each strain. Distance, duration, and speed proved to differ significantly between wild-type and mutant cells by $p < 0.001$, $p < 0.01$, and $p < 0.05$, respectively, using the nonparametric U-test.

DISCUSSION

Rationale of using RICM to wild-type and mutant cells

The first investigations on the interaction of *Dictyostelium* cells with a substratum by the use of RICM were conducted by Vince and Gingell (1980). In the present study the technique has been extended to cytoskeletal mutants and amended in two ways. First, by digital image processing the quality of the images has been improved and automatic extraction of quantitative data in real time has been achieved. Second, the introduction of freshly cleaved mica has proven to be crucial for discriminating details of cell behavior. The mica surface is extremely uniform and plain. Because the cells adhere only weakly to mica, this substratum is suited to accentuate subtle differences in cell adhesiveness.

We have concentrated in this study on cells in the preaggregation stage. When *D. discoideum* cells mature and acquire full aggregation competence, they tend to strongly elongate, and parameters recorded by RICM change accordingly (Igor Weber, pers. comm.).

Changes in the contact area reflect fluctuations in shape and motility of cells

The size of the contact area A_C of a single wild-type cell attached to mica has been shown to fluctuate with large amplitudes. Therefore, A_C can be used as a sensitive indicator for endogenous changes in the state of a cell. In particular, A_C data seem to monitor the functional state of the integral cortical region of a cell. As a scalar, A_C does not reflect changes in the directionality of locomotion or shape of cells, which have been analyzed using other parameters (Killich et al., 1993).

The observed A_C fluctuations are not obviously periodic, although our recordings are not long enough to exclude periodic components of low frequency on the order of minutes. In any case, the temporal pattern of A_C changes differs explicitly from oscillations in the adenylate cyclase activity. These oscillations give rise to pulses of cyclic AMP, a chemoattractant that is released from *D. discoideum* cells at regular intervals of about 6 min (Gerisch and Wick, 1975; Tomchik and Devreotes, 1981).

The A_C fluctuations might indicate deterministic chaotic behavior that results from nonlinear interactions in the mechanochemical control system of amoeboid cells. As seen in Figs. 6 and 9, there are phases of continuous A_C increase that span over more than a minute and, after a sharp turning point, phases of A_C decrease of similar length. These data indicate reactions in the cytoskeletal system that for a period of time drive the cell in one direction and, after a switch, into another direction.

The A_C fluctuations are associated with changes in cell shape and locomotion. It is possible, therefore, to relate the fluctuations recorded under our conditions to nonrandom features of cell locomotion previously observed in *Dictyostelium*. In trails of cells visualized on a surface that is coated with gold particles, phases of more or less straight movement alternate with curled paths (Kayman and Clarke, 1983). A characteristic of the locomotion of *Dictyostelium* cells is the suppression of pseudopod formation by an established leading edge. This suppression on the level of a single cell is formally equivalent to lateral inhibition in neuronal networks. It stabilizes the direction of locomotion in *Dictyostelium* cells, but is not as perfect as in keratocytes, which have a much more stable front region (Lee et al., 1993b). In *Dictyostelium*, new fronts are formed at intervals. Often these fronts successfully compete with the established ones, giving rise to an abrupt turn of locomotion. The degree of lateral inhibition is genetically determined in *D. discoideum*. Mutants with a defective control system have a high turning rate that corresponds to a more Brownian type of movement (Fisher et al., 1989).

Effects of the cytoskeleton on cell adhesion to a substratum

In an amoeboid cell, the plasma membrane is coupled to the subjacent network of actin filaments. It is this entity of plasma membrane and actin cortex that is primarily responsible for the shape and motility of the cells (for review, see

Sackmann, 1994). To explore the influence of the actin system on the interaction of cells with a substratum, we have used mutants in which defects in three proteins have been superimposed that are known to regulate in vitro either the cross-linkage or the length of actin filaments. By including triple mutants of different genetic origin in this study, the possibility that changes in membrane proteins or in constituents of the lipid bilayer due to mutations other than the known ones have been minimized. Therefore, alterations found in all these mutants can be attributed reliably to mutations in the genes for α-actinin, 120-kDa gelation factor, and severin.

An alteration consistently found in the triple mutants is a reduction in A_C, the size of the contact area. This effect depends on the surface to which cells of the triple mutants are exposed: it is not obvious on a clean glass surface, to which the cells adhere strongly, and is large on a mica surface, to which they adhere weakly. The conclusion is that high adhesion energy, as for the interaction of cells with glass, can compensate for the genetic defects in triple mutants that cause a decrease in the capability of forming contacts.

Alterations in pseudopod formation that are related to defects in cytoskeletal proteins

Typically, the formation of surface extensions in wild-type cells is characterized by a sudden onset, linear progression, and abrupt cessation (Fig. 11). This points to the presence of on and off switches in *Dictyostelium* cells, as they have been discussed for mammalian cells by Stossel (1993). In the triple mutants, pseudopods formed on the weakly adhesive mica surfaces are often short-lived and short in length (Table 3 and Fig. 12). This finding fits to previous notions that newly formed pseudopods can be stabilized in *Dictyostelium* cells by the cross-linkage of actin filaments (Condeelis, 1993) and also by contact with a substratum (Wessels et al., 1994). In a previous study with cells deficient in the 120-kDa cross-linking protein, a reduction in the number of pseudopods and in their speed of elongation has been reported (Cox et al., 1992). The bleb-like cell-surface extensions of our mutant cells (Figs. 9 and 10) are reminiscent of blebs formed by melanoma cells that lack the F-actin cross-linking protein filamin (Cunningham et al., 1992). The sequence of filamin is related to that of the 120-kDa gelation factor, one of the proteins missing in the triple mutants (Gorlin et al., 1990).

In *Dictyostelium*, cell surface blebbing is observed regularly in wild-type cells when the ATP concentration declines. Under these conditions, the actin cortex disrupts locally and the pressure imposed on the interior of the cell gives rise to blebs (Jungbluth et al., 1994). Subsequently, the cells round up and detach from the substratum. These results show that deviations of *Dictyostelium* cells from a spherical shape, which are necessary for appropriate adhesion to a plane surface, occur on the expense of ATP. Mutant cells lacking the conventional, double-headed myosin II have difficulty rounding up and detaching from a substratum after the inhibition of ATP synthesis (Pasternak et al., 1989), and they do not form blebs (G. Gerisch, unpublished observations). From these results, it is inferred that actin-myosin interactions in the cell cortex provide a major source of negative pressure that leads to bleb formation in *Dictyostelium* cells.

Severin, which is eliminated in the triple mutants together with the two actin-cross-linking proteins, cuts actin filaments and stays as a cap at the barbed ends of the fragments, thus inhibiting polymerization at the fast-growing ends (Yamamoto et al., 1982). It should be kept in mind, however, that actin-severin complexes act also as nuclei for filament growth at the pointed ends. In the theory of Oster and Perelson (1987), emphasis is placed on gel osmotic pressure as a basis of pseudopod protrusion. Because the osmotic pressure in an actin gel increases when filaments are cut, a function in pseudopod extension can be attributed to severin in the framework of this theory. In fact, stable overexpression of gelsolin, a homolog of severin, in fibroblasts increases the agonist-induced motility (Cunningham et al., 1991).

Because like gelsolin, severin is strictly Ca^{2+}-dependent, this protein might be sufficiently active only in cells that are subjected to stress or to stimuli that raise the cytoplasmic Ca^{2+} level. After microinjection of gelsolin into (unstimulated) fibroblasts or macrophages, no apparent effect has been observed, in contrast to microinjection of an NH_2-terminal fragment of gelsolin. This fragment, which severs actin filaments in a Ca^{2+}-independent fashion, causes disassembly of stress fibers and rounding up of the cells (Cooper et al., 1987). In light of these results, it is conceivable that circumstances strongly influence the role of severin in vivo: that elimination of severin has no substantial effect in *Dictyostelium* cells equipped with an otherwise normal cytoskeleton, as found by André et al. (1989), but has a pronounced effect in cells that suffer from a deficiency in the two actin-cross-linking proteins.

Because it is impossible to relate unequivocally the aberrant cell behavior found in triple mutants on mica to one of the actin-binding proteins that is missing in these mutants, the next step in analysis will be to study, by the RICM technique, mutant cells that lack only one or two of these proteins. Analysis of such mutants is in progress.

Theoretical considerations on differences between wild-type and mutant cells

Adhesion of a cell to a smooth surface requires a deformation of the plasma membrane. Theoretical considerations have demonstrated that transitions in the shape of soft shells such as lipid vesicles, caused by adhesion to a plane surface, are governed by competition between the adhesion energy and the bending energy of the vesicle membrane (Seifert and Lipowsky, 1990). As far as the envelope of *Dictyostelium* cells is concerned, not only the protein-lipid bilayer of the plasma membrane but also the subjacent actin cortex has to be considered.

A rigorous model would have to take into account that the cell shape is controlled by the bending stiffness and by the shear elasticity of the cell envelope. Both the stiffness and

elasticity depend on the coupling of the actin cortex to the protein-lipid bilayer membrane. But even if the shear elasticity is ignored, some features of the motion and adhesion of *Dictyostelium* cells can be explained in terms of the general minimum bending energy concept of the changes in shape that soft shells undergo when they adhere to a substratum. This concept predicts that the shape of adhering soft shells is determined by the minimum of the total free energy comprising four contributions:

(1) the curvature energy associated with the variation of the local curvature, which is characterized by the bending modulus K_C;
(2) the adhesion energy WA_C, where W is the adhesion energy per unit area;
(3) the work associated with a volume change caused by a pressure difference Δp ($=p_o - p_i$) between the outside (o) and the inside (i) of the cell, which can be expressed as $dW_v = \int \Delta p dV$;
(4) the extensional energy, arising if the average area $\langle A \rangle$ of the cell membrane is changed, which may be expressed as $\Sigma \oint dA$, where Σ is the membrane tension and the integral extends over the total surface area of the cell.

The pressure difference in (3) may be due to osmotic pressure or may be generated by contraction or expansion of the actin network, most likely involving myosin II. The lateral tension in (4) is maintained by the triple-layered cell envelope, and the resistance toward area changes depends sensitively on the state of its three leaflets, the membrane bilayer, and the actin cortex. If the bilayer exhibits a larger area than the cytoskeleton, the membrane tension, Σ, is dominated by the actin cortex because the bilayer tension is determined by the thermally excited bending undulations and is very small. However, if the bilayer is fully expanded, Σ is very large because of the extremely small lateral compressibility of lipid bilayers (Evans and Needham, 1986). The maximum degree of cell spreading is thus determined by the area of the bilayer membrane, which could be expanded, of course, by fusion of cytoplasmatic vesicles.

According to the minimum bending energy concept, the shape of adhering shells and, thus, the contact area A_C depend on three reduced parameters:

$$p = \frac{\Delta p}{K_C R^2}, \qquad \sigma = \frac{\Sigma R^2}{K_C} \qquad \text{and} \qquad w = \frac{WR^2}{K_C},$$

where R (called "equivalent radius") is the radius of a sphere exhibiting the same volume as the cell. Calculations of the shape and contact area as a function of the control parameters p, σ, and w show two important consequences of the model.

(1) For a given reduced adhesion energy w, the contact area A_C decreases roughly linearly with increasing pressure difference p. A change in K_C alone would lead only to second-order changes of the contact area. This may be one reason for the small effects of cytoskeletal mutations on cell locomotion.
(2) At pressure equilibrium ($\Delta p = 0$), the cell membrane is expected to exhibit thermally excited bending undulations as known from erythrocyte studies (Zilker et al., 1992). These undulations lead to a repulsive force that can be as strong as the van der Waals attraction and thus may reduce w substantially. This has been discussed by Seifert and Lipowsky (1990) and experimentally studied by Rädler et al. (1994) for bilayered lipid vesicles. The amplitude of these undulations and the arising repulsive force depend inversely on the membrane tension and the bending stiffness. Therefore, it is possible that a transition from a state with a large contact area to a state with a small area can be induced not only by increasing but also by decreasing the bending stiffness. To estimate the negative contribution of thermally excited undulations to the adhesion energy of living, motile cells, more experimental data on such cells are required.

The effective bending stiffness of the triple-layered cell envelope will be changed dramatically by variation of the degree of coupling between the lipid bilayer and the actin layer. This means that a transition in cell shape and a decrease in the size of the contact area can be brought about either by decreasing the degree of cross-linkage within the actin cortex or by decreasing the degree of its coupling to the membrane bilayer. A complication is introduced if in a moving cell the composite membrane becomes nonisotropic with respect to lateral organization and deformability. In particular, the degree of bilayer-cytoskeleton coupling may not be the same in the free cell envelope and the area of cell contact with a substratum.

Applied to *Dictyostelium*, the minimum bending energy concept predicts that the bleb-like extensions of mutant cells and the reduced size of their contact areas may result from a decrease in the bending stiffness caused by the lack of two actin-cross-linking proteins. According to the theory, the temporal changes in cell shape and A_C, as they have been observed in wild-type and mutant cells, may be brought about by variations in the coupling between the lipid protein-bilayer and the actin cortex and/or by variations in the pressure difference.

Because myosin II appears to contribute strongly to the pressure difference in *Dictyostelium* cells, the observed temporal changes in cell shape and adhesion might be based on fluctuations of the myosin activity. A common mechanism for the regulation of myosin activities is phosphorylation. The contribution of myosin II to the observed variations in cell behavior are testable by assaying myosin II null mutants (Manstein et al., 1989) or mutants defective in myosin II phosphorylation (Egelhoff et al., 1993; Gerisch et al., 1993) by the RICM technique.

We are very grateful to Drs. Ken Jacobson, Elliot Elson, and Mike Sheetz for valuable discussions. M. Schindl thanks Dr. Albert Harris for advice and encouragement.
This work was supported by the Deutsche Forschungsgemeinschaft (SFB 266) and by the "Fonds der Chemischen Industrie."

REFERENCES

André, E., M. Brink, G. Gerisch, G. Isenberg, A. Noegel, M. Schleicher, J. E. Segall, and E. Wallraff. 1989. A *Dictyostelium* mutant, deficient in severin, an F-actin fragmenting protein, shows normal motility and chemotaxis. *J. Cell Biol.* 108:985–995.

Bayley, S. W. 1984. Classification and structures of the micas. *Rev. Mineral.* 13:1–12.

Brink, M., G. Gerisch, G. Isenberg, A. A. Noegel, J. E. Segall, E. Wallraff, and M. Schleicher. 1990. A *Dictyostelium* mutant lacking an F-actin cross-linking protein, the 120-kD gelation factor. *J. Cell Biol.* 111:1477–1489.

Brown, S. S., K. Yamamoto, and J. A. Spudich. 1982. A 40,000-Dalton protein from *Dictyostelium discoideum* affects assembly properties of actin in a Ca^{2+}-dependent manner. *J. Cell Biol.* 93:205–210.

Cohen, M. H., and A. Robertson. 1971. Chemotaxis and the early stages of aggregation in cellular slime molds. *J. Theor. Biol.* 31:119–130.

Condeelis, J. 1993. Life at the leading edge: the formation of cell protrusions. *Annu. Rev. Cell Biol.* 9:411–444.

Condeelis, J., and M. Vahey. 1982. A calcium- and pH-regulated protein from *Dictyostelium discoideum* that cross-links actin filaments. *J. Cell Biol.* 94:466–471.

Condeelis, J., M. Vahey, J. M. Carboni, J. DeMey, and S. Oghihara. 1984. Properties of the 120,000- and 95,000-dalton actin-binding proteins from *Dictyostelium discoideum* and their possible functions in assembling the cytoplasmic matrix, *J. Cell Biol.* 99(Suppl.):119s–126s.

Cooper, J. A., J. Bryan, B. Schwab III, C. Frieden, D. J. Loftus, and E. L. Elson. 1987. Microinjection of gelsolin into living cells. *J. Cell Biol.* 104:491–501.

Cox, D., J. Condeelis, D. Wessels, D. Soll, H. Kern, and D. A. Knecht. 1992. Targeted disruption of the ABP-120 gene leads to cells with altered motility. *J. Cell Biol.* 116:943–955.

Cunningham, C. C., J. B. Gorlin, D. J. Kwiatkowski, J. H. Hartwig, P. A. Janmey, H. R. Byers, and T. P. Stossel. 1992. Actin-binding protein requirement for cortical stability and efficient locomotion. *Science.* 255:325–327.

Cunningham, C. C., T. P. Stossel, and D. J. Kwiatkowski. 1991. Enhanced motility in NIH 3T3 fibroblasts that overexpress gelsolin. *Science.* 251: 1233–1236.

Curtis, A. S. G. 1964. The mechanism of adhesion of cells to glass. A study by interference reflection microscopy. *J. Cell Biol.* 20:199–215.

de Hostos, E. L., C. Rehfueß, B. Bradtke, D. R. Waddell, R. Albrecht, J. Murphy, and G. Gerisch. 1993. *Dictyostelium* mutants lacking the cytoskeletal protein coronin are defective in cytokinesis and cell motility. *J. Cell Biol.* 120:163–173.

De Lozanne, A., and J. A. Spudich. 1987. Disruption of the *Dictyostelium* myosin heavy chain gene by homologous recombination. *Science.* 236: 1086–1091.

Devreotes, P. N., and S. H. Zigmond. 1988. Chemotaxis in eukaryotic cells: a focus on leukocytes and *Dictyostelium*. *Annu. Rev. Cell Biol.* 4:649–686.

Dunn, G. A., and A. F. Brown. 1990. Quantifying cellular shape using moment invariants. Lecture notes in biomathematics. *Biological Motion.* 89:10–34.

Egelhoff, T. T., R. J. Lee, and J. A. Spudich. 1993. *Dictyostelium* myosin heavy chain phosphorylation sites regulate myosin filament assembly and localization in vivo. *Cell.* 75:363–371.

Evans, E. 1993. New physical concepts for cell amoeboid motion. *Biophys.J.* 64:1306–1322.

Evans, E., and D. Needham. 1986. Long range interactions between lipid bilayers in salt solutions and solutions of non-adsorbant polymers: comparison of mean-field theory with direct measurements. *Faraday Dis. Chem. Soc.* 81:267.

Fisher, P. R., R. Merkl, and G. Gerisch. 1989. Quantitative analysis of cell motility and chemotaxis in *Dictyostelium discoideum* by using an image processing system and a novel chemotaxis chamber providing stationary chemical gradients. *J. Cell Biol.* 108:973–984.

Futrelle, R. P., J. Traut, and W. G. McKee. 1982. Cell behavior in *Dictyostelium discoideum*: preaggregation response to localized cyclic AMP pulses. *J. Cell Biol.* 92:807–821.

Gerisch, G., R. Albrecht, E. de Hostos, E. Wallraff, C. Heizer, M. Kreitmeier, and A. Müller-Taubenberger. 1993. Actin-associated proteins in motility and chemotaxis of *Dictyostelium* cells. *In* Cell Behaviour: Adhesion and Motility. G. Jones, C. Wigley, and R. Warn, editors. *Soc. Exp. Biol. Symp.* 47:297–315.

Gerisch, G., and H. U. Keller. 1981. Chemotactic reorientation of granulocytes stimulated with micropipettes containing fMet-Leu-Phe. *J. Cell Sci.* 52:1–10.

Gerisch, G., and U. Wick. 1975. Intracellular oscillations and release of cyclic AMP from *Dictyostelium* cells. *Biochem. Biophys. Res. Commun.* 65:364–370.

Gingell, D., and I. Todd. 1979. Interference reflection microscopy. A quantitative theory for image interpretation and its application to cell-substratum separation measurements. *Biophys. J.* 26:507–526.

Gingell, D., I. Todd, and O. S. Heavens. 1982. Quantitative interference microscopy: effect of microscope aperture. *Optica Acta.* 29: 901–908.

Gorlin, J. B., R. Yamin, S. Egan, M. Stewart, T. P. Stossel, D. J. Kwiatkowski, and J. H. Hartwig. 1990. Human endothelial actin-binding protein (ABP-280, nonmuscle filamin): a molecular leaf spring. *J. Cell Biol.* 111:1089–1105.

Harris, A. K., P. Wild, and D. Stopak. 1980. Silicone rubber substrata: a new wrinkle in the study of cell locomotion. *Science.* 208:177–179.

Isenberg, G., and W. H. Goldmann. 1992. Actin-membrane coupling: a role for talin. *J. Muscle Res. Cell Motil.* 13:587–589.

Janmey, P. A. 1991. Mechanical properties of cytoskeletal polymers. *Curr. Opin. Cell Biol.* 2:4–11.

Janmey, P. A., S. Hvidt, J. Lamb, and T. P. Stossel. 1990. Resemblance of actin-binding protein/actin gels to covalently crosslinked networks. *Nature.* 345:89–92.

Jung, G., and J. A. Hammer III. 1990. Generation and Characterization of *Dictyostelium* cells deficient in a myosin I heavy chain isoform. *J. Cell Biol.* 110:1955–1964.

Jungbluth, A., V. von Arnim, E. Biegelmann, B. Humbel, A. Schweiger, and G. Gerisch. 1994. Strong increase in the tyrosine phosphorylation of actin upon inhibition of oxidative phosphorylation: correlation with reversible rearrangements in the actin skeleton of *Dictyostelium* cells. *J. Cell Sci.* 107:117–125.

Kayman, S. C., and M. Clarke. 1983. Relationship between axenic growth of *Dictyostelium discoideum* strains and their track morphology on substrates coated with gold particles. *J. Cell Biol.* 97:1001–1010.

Killich, T., P. J. Plath, X. Wei, H. Bultmann, L. Rensing, and M. G. Vicker. 1993. The locomotion, shape and pseudopodial dynamics of unstimulated *Dictyostelium* cells are not random. *J. Cell Sci.* 106:1005–1013.

Knecht, D. A., and W. F. Loomis. 1987. Antisense RNA inactivation of myosin heavy chain gene expression in *Dictyostelium discoideum. Science.* 236:1081–1086.

Kolodney, M. S., and E. L. Elson. 1993. Correlation of myosin light chain phosphorylation with isometric contraction of fibroblasts. *J. Biol. Chem.* 268:23850–23855.

Lee, J., A. Ishihara, and K. Jacobson. 1993a. How do cells move along surfaces? *Trends Cell Biol.* 3:366–370.

Lee, J., A. Ishihara, J. A. Theriot, and K. Jacobson. 1993b. Principles of locomotion for simple-shaped cells. *Nature.* 362:167–171.

Manstein, D. J., M. A. Titus, A. De Lozanne, and J. A. Spudich. 1989. Gene replacement in *Dictyostelium*: generation of myosin null mutants. *EMBO J.* 8:923–932.

Metz, B. A., T. E. Ward, D. L. Welker, and K. L. Williams. 1983. Identification of an endogenous plasmid in *Dictyostelium discoideum. EMBO J.* 2:515–519.

Müller, O., H. E. Gaub, M. Bärmann, and E. Sackmann. 1991. Viscoelastic moduli of sterically and chemically cross-linked actin networks in the dilute to semidilute regime: measurements by an oscillating disk rheometer. *Macromolecules.* 24:3111–3120.

Newell, P. C. 1982. Genetics. *In* The Development of *Dictyostelium discoideum.* W. F. Loomis, editor. Academic Press, New York. 35–70.

Noegel, A. A., S. Rapp, F. Lottspeich, M. Schleicher, and M. Stewart. 1989. The *Dictyostelium* gelation factor shares a putative actin binding site with α-actinins and dystrophin and also has a rod domain containing six 100-residue motifs that appear to have a cross-beta conformation. *J. Cell Biol.* 109:607–618.

Oster, G. F., and A. S. Perelson. 1987. The physics of cell motility. *J. Cell Sci.* 8:35–54.

Pasternak, C., J. A. Spudich, and E. L. Elson. 1989. Capping of surface receptors and concomitant cortical tension are generated by conventional myosin. *Nature*. 341:549–551.

Ploem, J. S. 1975. Reflection-contrast microscopy as a tool for investigation of the attachment of living cells to a glass surface. *In* Mononuclear Phagocytes in Immunity, Infection and Pathology. R. V. Furth, editor. Blackwell Scientific Publications, Oxford.

Radmacher, M. 1991. Diploma thesis. Technische Universität München. 76 pp.

Rädler, J., and E. Sackmann. 1992. On the measurement of weak repulsive and frictional colloidal forces by reflection interference contrast microscopy. *Langmuir*. 8:848–853.

Rädler, J., and E. Sackmann. 1993. Imaging optical thicknesses and separation distances of phospholipid vesicles at solid surfaces. *J. Phys. II France*. 3:727–748.

Rädler, J. O., T. J. Feder, H. H. Strey, and E. Sackmann. 1995. Fluctuation analysis of tension-controlled undulation forces between giant vesicles and solid substrates. *Phys. Rev. E*. In press.

Rossier, C., G. Gerisch, D. Malchow, and F. Eckstein. 1978. Action of a slowly hydrolysable cyclic AMP analogue on developing cells of *Dictyostelium discoideum*. *J. Cell Sci.* 35:321–338.

Ruddies, R., W. H. Goldmann, G. Isenberg, and E. Sackmann. 1993. The viscoelasticity of entangled actin networks: the influence of defects and modulation by talin and vinculin. *Eur. Biophys. J.* 22:309–321.

Sackmann, E. 1994. Intra- and extracellular macromolecular networks: physics and biological function. *Macromol. Chem. Phys.* 195:7–28.

Schleicher, M., A. Noegel, T. Schwarz, E. Wallraff, M. Brink, J. Faix, G. Gerisch, and G. Isenberg. 1988. A *Dictyostelium* mutant with severe defects in α-actinin: its characterization using cDNA probes and monoclonal antibodies. *J. Cell Sci.* 90:59–71.

Seifert, U., and R. Lipowsky. 1990. Adhesion of vesicles. *Phys. Rev. A*. 42:4768–4771.

Stossel, T. P. 1993. On the crawling of animal cells. *Science*. 260: 1086–1094.

Taylor, D. L., and J. S. Condeelis. 1979. Cytoplasmic structure and contractility in amoeboid cells. *Int. Rev. Cytol.* 56:57–144.

Titus, M. A., D. Wessels, J. A. Spudich, and D. Soll. 1993. The unconventional myosin encoded by the *myo*A gene plays a role in *Dictyostelium* motility. *Mol. Biol. Cell*. 4:233–246.

Tomchik, K. J., and P. N. Devreotes. 1981. Adenosine 3′,5′-monophosphate waves in *Dictyostelium discoideum*: a demonstration by isotope dilution-fluorography. *Science*. 212:443–446.

Verschueren, H. 1985. Interference reflection microscopy in cell biology: methodology and applications. *J. Cell Sci.* 75:279–301.

Vince, S., and D. Gingell. 1980. Cationic modulation of the interaction of *Dictyostelium discoideum* amoebae with glass. Evidence from quantitative interference reflection microscopy. *Exp. Cell Res.* 126:462–465.

Wallraff, E., and G. Gerisch. 1991. Screening for *Dictyostelium* mutants defective in cytoskeletal proteins by colony immunoblotting. *Methods Enzymol.* 196:334–348.

Wallraff, E., M. Schleicher, M. Modersitzki, D. Rieger, G. Isenberg, and G. Gerisch. 1986. Selection of *Dictyostelium* mutants defective in cytoskeletal proteins: use of an antibody that binds to the ends of α-actinin rods. *EMBO J.* 5:61–67.

Wallraff, E., D. L. Welker, K. L. Williams, and G. Gerisch. 1984. Genetic analysis of a *Dictyostelium discoideum* mutant resistant to adenosine-3′:5′-cyclic phosphorothioate, an inhibitor of wild-type development. *J. Gen. Microbiol.* 130:2103–2114.

Welker, D. L., and K. L. Williams. 1980. Mitotic arrest and chromosome doubling using thiabendazole, cambendazole, nocodazole and benlate in the slime mould *Dictyostelium discoideum*. *J. Gen. Microbiol.* 116:397–407.

Wessels, D., N. A. Schroeder, E. Voss, A. L. Hall, J. Condeelis, and D. R. Soll. 1989. cAMP-mediated inhibition of intracellular particle movement and actin reorganization in Dictyostelium, *J. Cell Biol.* 109:2841–2851.

Wessels, D., H. Vawter-Hugart, J. Murray, and D. R. Soll. 1994. Three-dimensional dynamics of pseudopod formation and the regulation of turning during the motility cycle of *Dictyostelium*. *Cell Motil. Cytoskel.* 27: 1–12.

Williams, K. L. 1978. Characterization of dominant resistance to cobalt chloride in *Dictyostelium discoideum* and its use in parasexual genetic analysis. *Genetics*. 90:37–47.

Williams, K. L., and P. C. Newell. 1976. A genetic study of aggregation in the cellular slime mould *Dictyostelium discoideum* using complementation analysis. *Genetics*. 82:287–307.

Witke, W., W. Nellen, and A. Noegel. 1987. Homologous recombination in the *Dictyostelium* α-actinin gene leads to an altered mRNA and lack of the protein. *EMBO J.* 6:4143–4148.

Witke, W., M. Schleicher, and A. A. Noegel. 1992. Redundancy in the microfilament system: abnormal development of *Dictyostelium* cells lacking two F-actin cross-linking proteins. *Cell*. 68:53–62.

Yamamoto, K., J. D. Pardee, J. Reidler, L. Stryer, and J. A. Spudich. 1982. Mechanism of interaction of *Dictyostelium* severin with actin filaments. *J. Cell Biol.* 95:711–719.

Zilker, A., H. Engelhardt, and E. Sackmann. 1987. Dynamic reflection interference contrast (RIC-) microscopy: a new method to study surface excitations of cells and to measure membrane bending elastic moduli. *J. Phys. France*. 48:2139–2151.

Zilker, A., M. Ziegler, and E. Sackmann. 1992. Spectral analysis of erythrocyte flickering in the 0.3–4-μm^{-1} regime by microinterferometry combined with fast image processing. *Phys. Rev. A*. 46:7998—8001.